**ADVANCED
MATERIALS
TECHNOLOGIES**

Supporting Information

Turning Trash into Treasure: MXene with Intrinsic LiF Solid Electrolyte Interfaces Performs Better and Better during Battery Cycling

Hao Xu, Wen Zhu, Fengzhan Sun, Hu Qi, Jianxin Zou,* Richard Laine,* and Wenjiang Ding

Turning Trash into Treasure: MXene with Intrinsic LiF Solid Electrolyte Interfaces Performs Better and Better during Battery Cycling

Hao Xu, Wen Zhu, Fengzhan Sun, Hu Qi, Jianxin Zou*, Richard Laine* and Wenjiang Ding

Supporting Information

Turning Trash into Treasure: MXene with Intrinsic LiF Solid Electrolyte Interfaces Performs Better and Better during Battery Cycling

Hao Xu, Wen Zhu, Fengzhan Sun, Hu Qi, Jianxin Zou*, Richard Laine** and Wenjiang Ding

H. Xu, W. Zhu, F. Z. Sun, H. Qi, Prof. J. X. Zou, Prof. W. J. Ding
National Engineering Research Center of Light Alloy Net Forming
School of Materials Science and Engineering
Shanghai Jiao Tong University
Shanghai, 200240, P. R. China
E-mail: zoujx@sjtu.edu.cn
H. Xu, W. Zhu, F. Z. Sun, H. Qi, Prof. J. X. Zou, Prof. W. J. Ding
State Key Laboratory of Metal Matrix Composites
School of Materials Science and Engineering
Shanghai Jiao Tong University
Shanghai, 200240, P. R. China
H. Xu, W. Zhu, F. Z. Sun, H. Qi, Prof. J. X. Zou, Prof. W. J. Ding
Center of Hydrogen Science
Shanghai Jiao Tong University
Shanghai, 200240, P. R. China
Prof. R. M. Laine
Department of Materials Science and Engineering
University of Michigan, Ann Arbor
Michigan 48109-2136, United States
E-mail: talsdad@umich.edu

EXPERIMENTAL SECTION

1. Preparation for *m*-Ti$_3$C$_2$/LiF(S$_1$), *m*-Ti$_3$C$_2$/MgF$_2$(S$_2$) and Ti$_3$C$_2$.

In a special experiment, 1.6 g lithium fluoride (LiF, >99.99 wt. %, Aladdin Reagent) powder was immersed in 30 mL concentrated hydrochloric acid (HCl, ~40 wt. %, Aladdin Reagent). The samples were mixed and stirred at 600 rpm for 5 minutes. Then, 1 g commercially available Ti$_3$AlC$_2$ (>98 wt. %, Forsman Technology Co. Ltd., Beijing) was gradually added to the above samples over the course of 5min to avoid overheating, followed by continuously stirring at 600 rpm and reacting at 40 °C for 45 h. The reaction products were washed with deionized water and centrifuged for many times at 4000 rpm until the pH value of the supernatant reached approximately 6. After that, the products were under sonication for 1.5 h followed by centrifugation at 10000 rpm for 10 min. The dark green supernatant was then decanted, to obtain single-layered Ti$_3$C$_2$ (s-Ti$_3$C$_2$) after freeze-drying. Then, the sediments were dried in the vacuum oven at 60 °C. Subsequently, multilayered Ti$_3$C$_2$/LiF sediments [denoted as *m*-Ti$_3$C$_2$/LiF(S$_1$)] were obtained. To prepare the multilayered Ti$_3$C$_2$/MgF$_2$ sediments [denoted as *m*-Ti$_3$C$_2$/MgF$_2$(S$_2$)], all conditions were the same except for that 1.6 g lithium fluoride was changed to 1.9 g magnesium fluoride (MgF$_2$, > 99.9 wt. %, Aladdin Reagent). To obtain sole Ti$_3$C$_2$, 1g Ti$_3$AlC$_2$ reacted with 30 mL hydrofluoric acid (HF, ~40 wt. %, Aladdin Reagent) followed by stirring (600 rpm) at 40 °C for 45 h. The subsequent procedure is consistent with that for synthesis of *m*-Ti$_3$C$_2$/LiF(S$_1$).

2. Electrochemical measurements

The coin-type cells (CR2032) were assembled in an argon-filled glove box with the content of water and oxygen less than 0.1 ppm. To fabricate working anodes, the

as-obtained active materials were mixed with PVDF and super P carbon black at a mass ratio of 8:1:1. Then the NMP was added to the above mixture to form a slurry, uniformly pasted on the surface of the copper foil for vacuum drying at 120 ℃ for 8 h. The mass loading of active material is 0.8-1.2 mg cm^{-2}. Metallic Li foil was made as the anode and the microporous polyethylene membrane (Celgard 2400) was posted as the separator. The mixtures of 1M LiPF$_6$ in the solvent containing ethylene carbonate, diethyl carbonate and dimethyl carbonate (EC/DEC/DMC, 1:1:1 at volume ratio) were used as the electrolyte.

A LAND CT2001A multichannel battery test system between 0.01 and 3 V vs Li$^+$/Li at 25 ℃ was used for the galvanostatic charge/discharge cycling tests. Cyclic voltammetry (CV) test with different sweep rates between 0.1 and 0.8 mV s^{-1} and electrochemical impedance spectroscopy (EIS) with amplitude of 5mV and frequency between 100 kHz and 0.01Hz were implemented on an electrochemical workstation (CHI 660E, Chenhua).

3. Material characterization

X-ray diffraction (XRD) was implemented on a Rigaku Smart Lab diffractometer with Cu-Kα radiation (λ=1.5406 Å) at a scanning rate 5° min^{-1}. The morphologies of the products were examined by scanning electron microscopy (SEM, Phenom XL and Mira 3), transmission electron microscopy (TEM, Talos F200X). Energy dispersive X-ray (EDX) spectrometer was attached on SEM. Selected area electron diffraction (SAED) and high resolution transmission electron microscopy (HRTEM) were performed on a Talos F200X microscopy with an accelerating voltage of 200 kV. The

electrodes after different cycles in fully charged state were dismantled in the glove box with the content of water and oxygen both less than 0.1 ppm, then to be dried in the vacuum oven at 30°C for 2h. The electrodes were directly conducted in SEM and XRD measurements. The elemental valence was characterized by X-ray photoelectron spectroscopy equipped with a monochromated Al-Kα X-ray source (XPS, Ultra DLD, 1486.7 eV). 284.8 eV was used for C 1s as the reference to calibrate the XPS data. Besides, peak fitting was done using CASA XPS software.
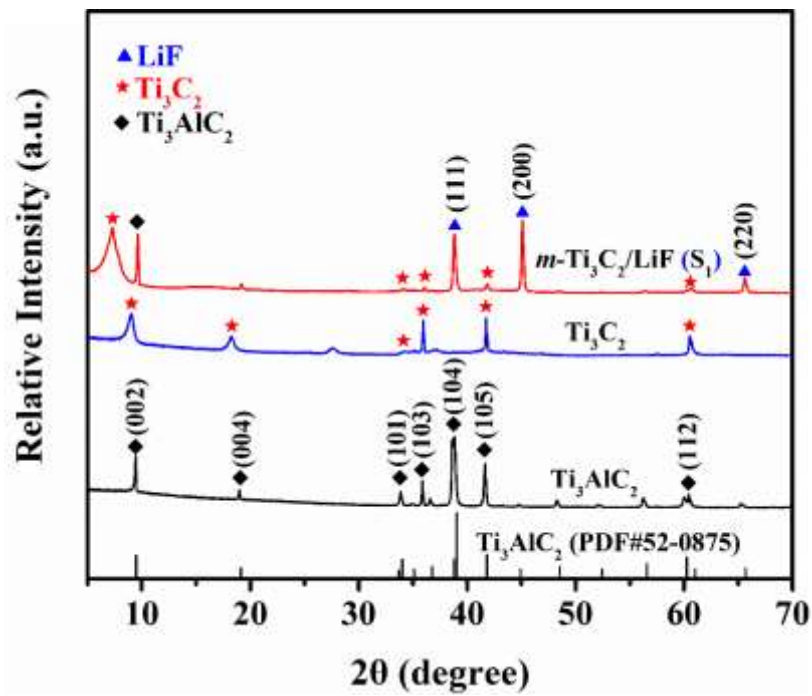
Figure S1. XRD of Ti_3C_2, Ti_3AlC_2 and m-Ti_3C_2/LiF(S_1).
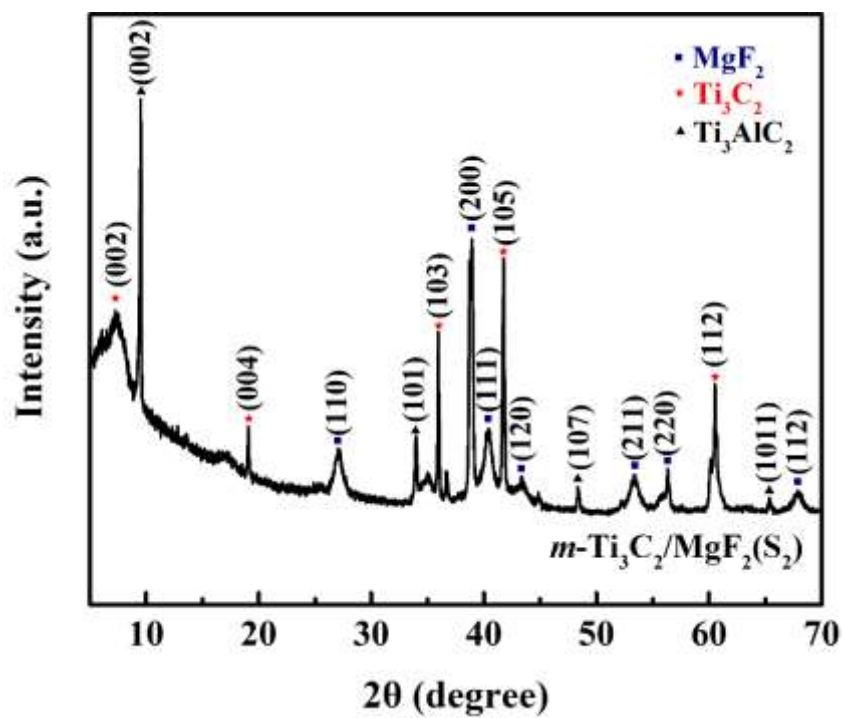
Figure S2. XRD of *m*-Ti₃C₂/MgF₂(S₂).
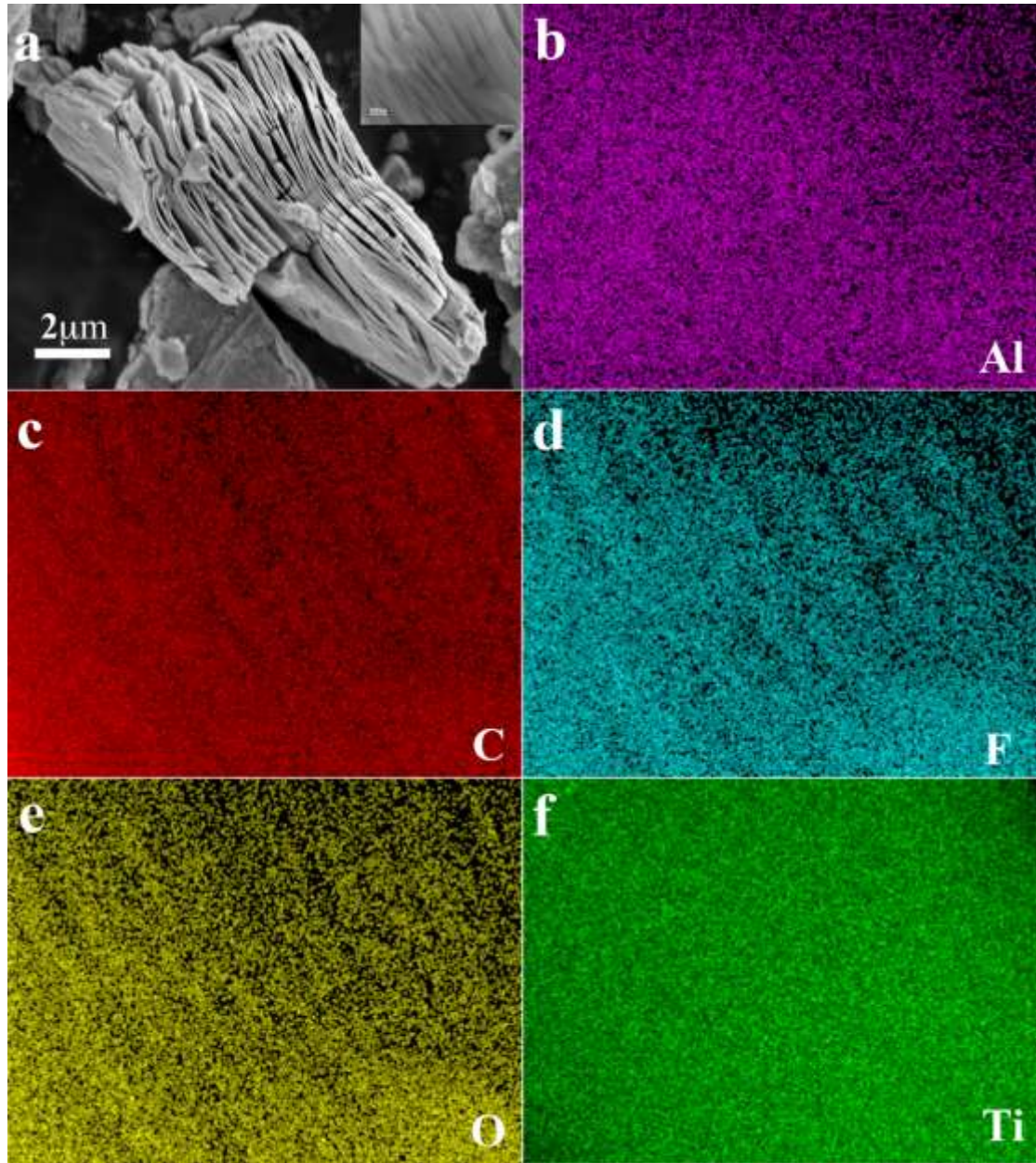
Figure S3. SEM and EDX of Ti_3C_2 etched by HF.
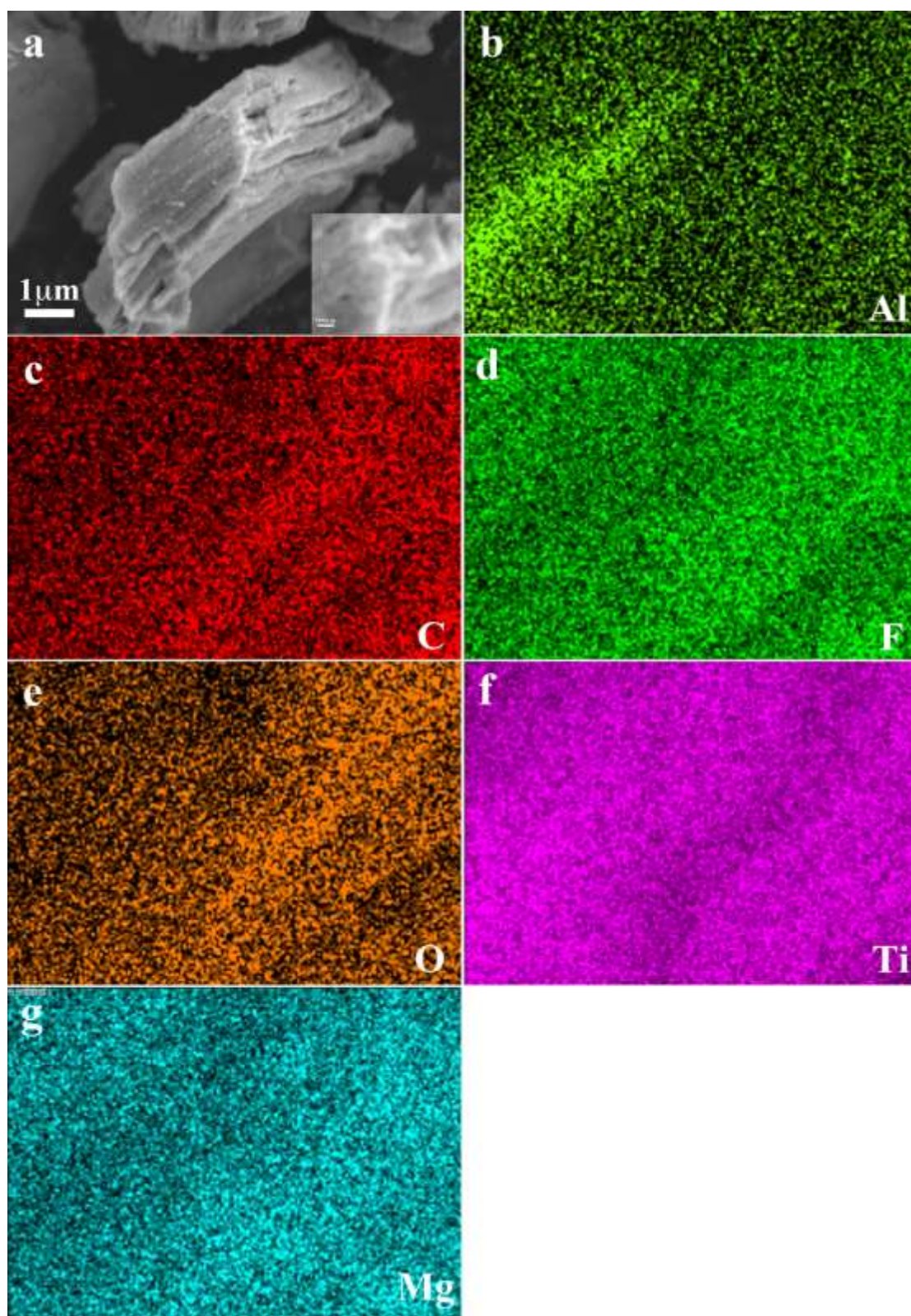
Figure S4. SEM and EDX of $Ti_3C_2/MgF_2(S_2)$ etched by HCl and MgF_2.
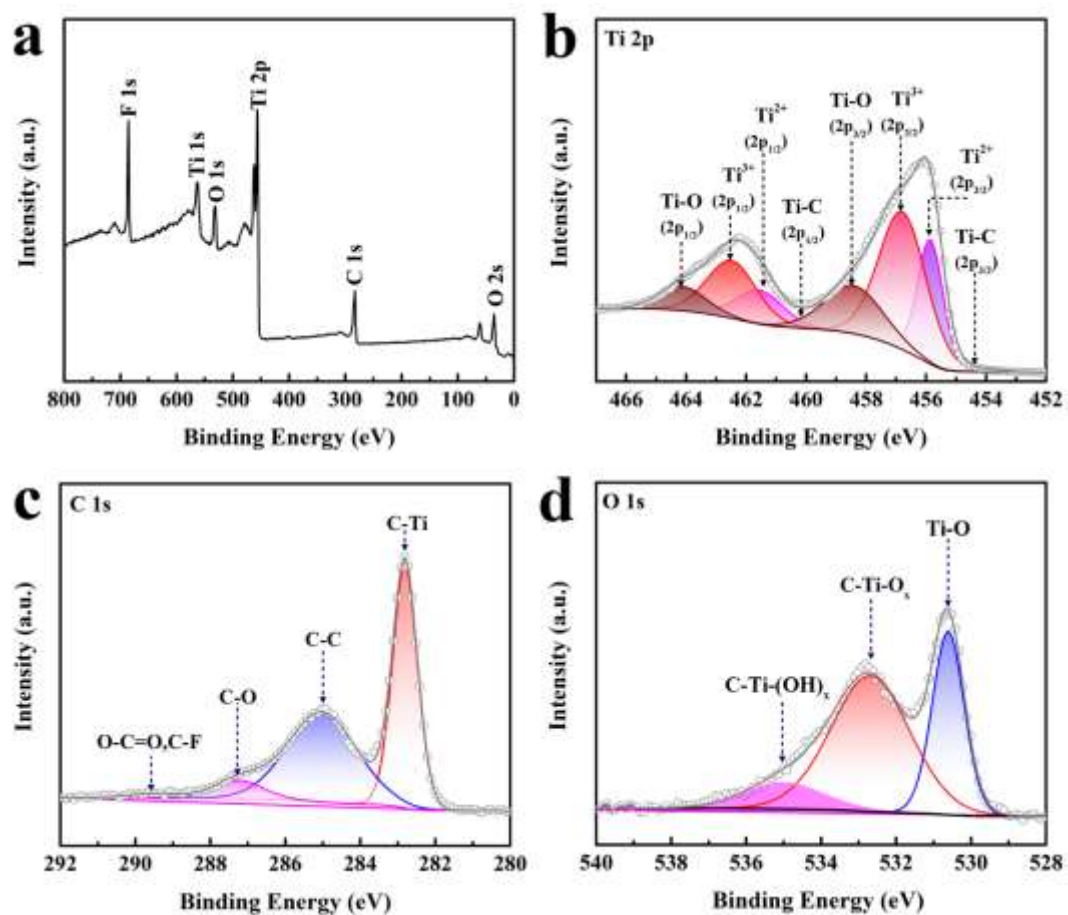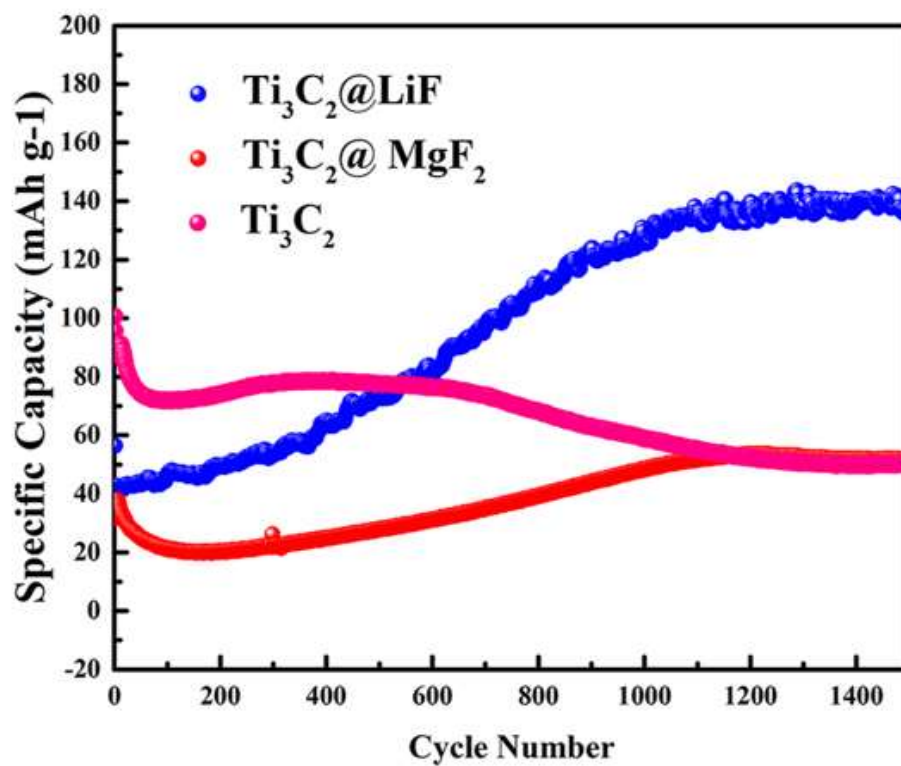
Figure S5. XPS spectra of Ti_3C_2 etched by HF. a) Survey spectrum, b) Ti 2p, c) C 1s and d) O 1s.
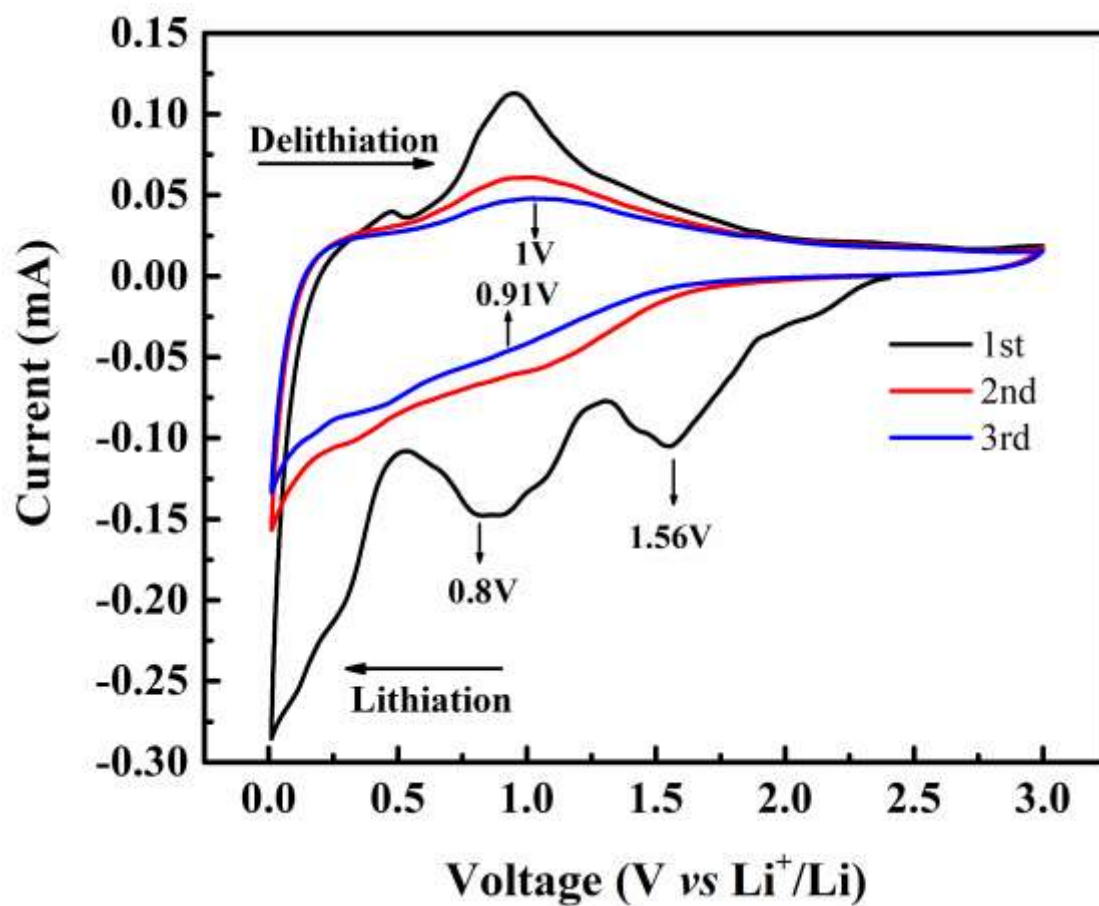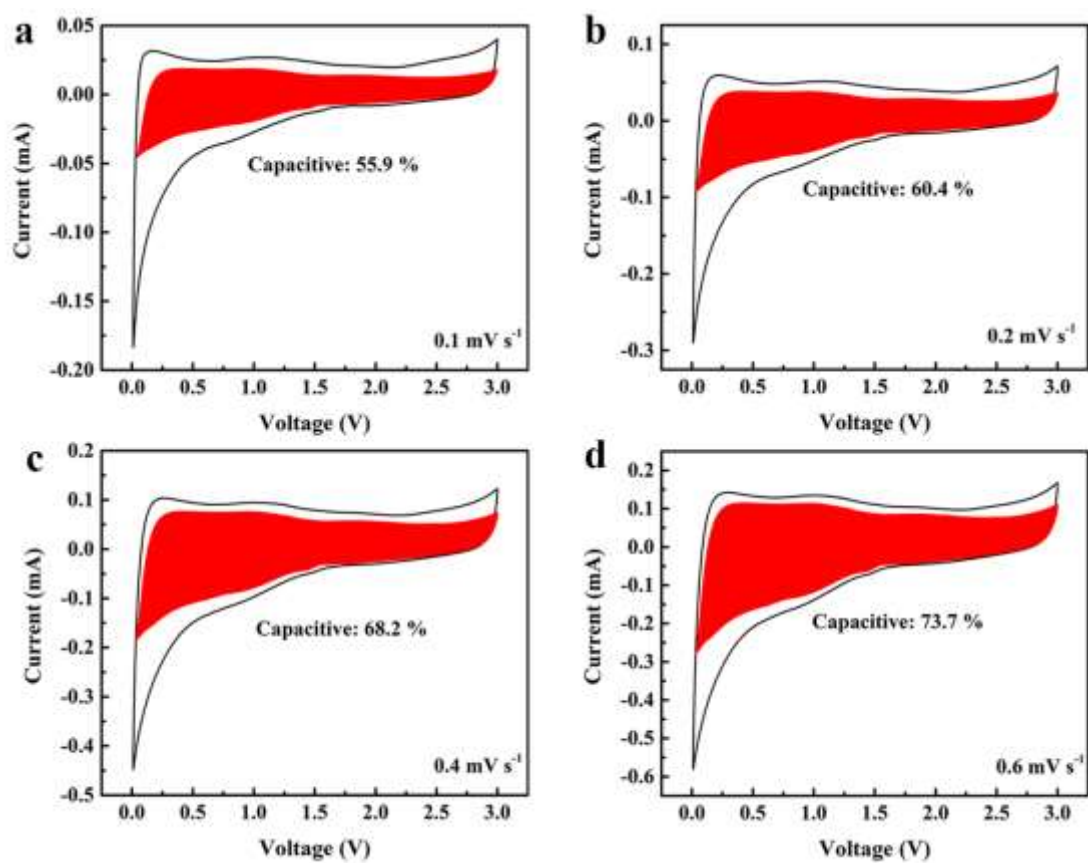
Figure S6. CV curves of Ti_3C_2 etched by HF for LIB at 0.1mV s^{-1} for the first three cycles.
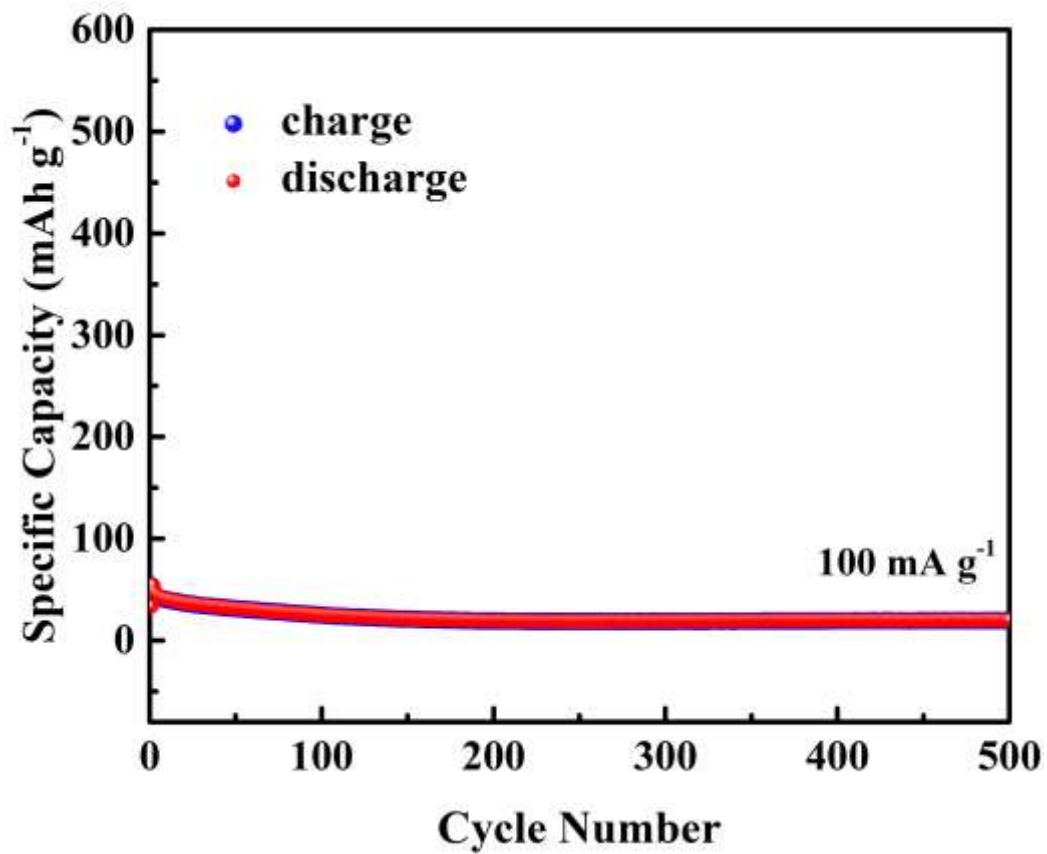
Figure S7. Long-term cycling performance LiF for LIBs at 100 mA g^{-1}.

Figure S8. Long-term cycling performance of m-Ti$_3$C$_2$/LiF(S$_1$), m-Ti$_3$C$_2$/MgF$_2$(S$_2$) and Ti$_3$C$_2$ for LIBs at 300 mA g^{-1}.

Figure S9. CV curves with corresponding capacitive contribution at a) 0.1, b) 0.2, c) 0.4 and d) 0.6 mV s^{-1} of m-Ti$_3$C$_2$/LiF(S$_1$) after 1000 cycles at 300 mA g^{-1}.
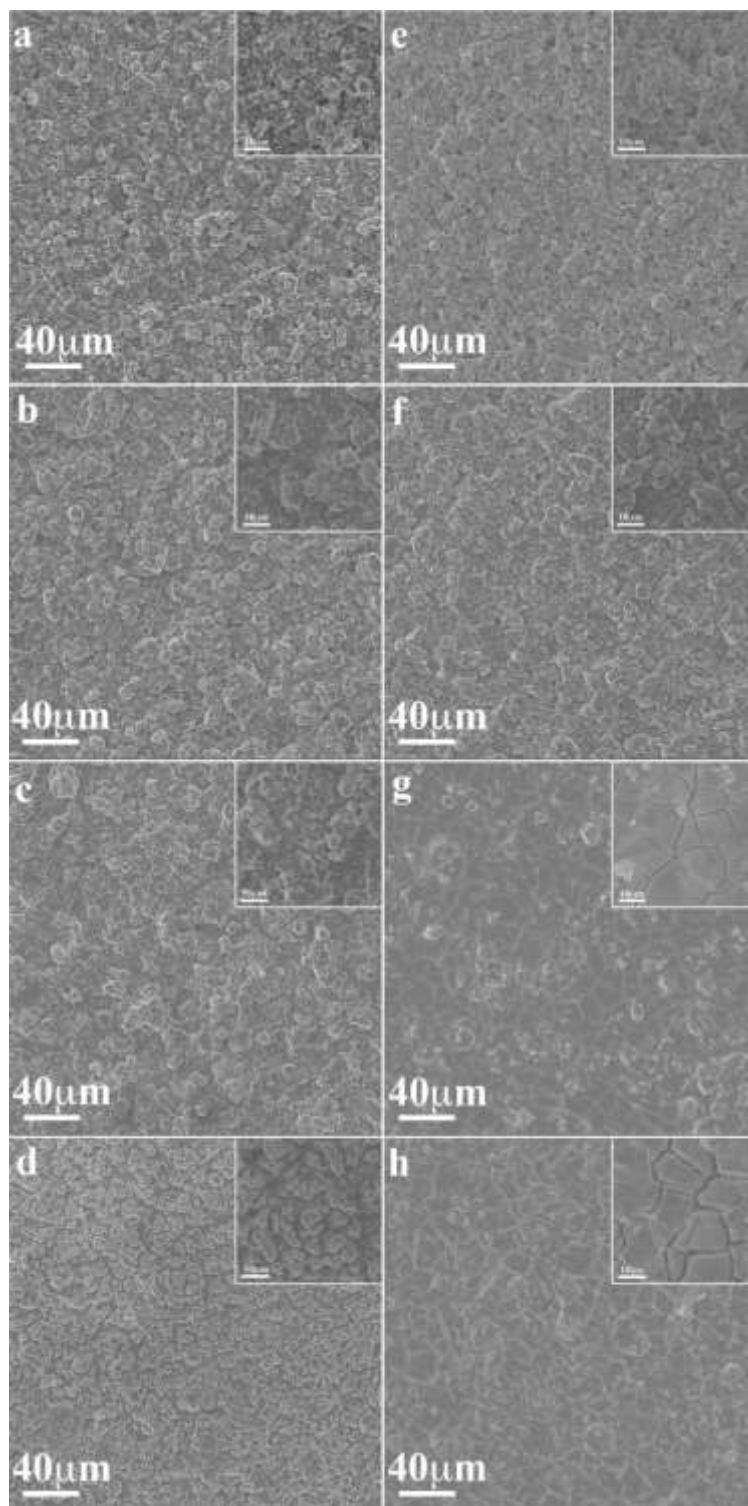
Figure S10. Front SEM images of the electrodes in fully charged state. a) Fresh electrode, electrodes after b) 200, c) 600, d) 1200 cycles at 300mA g^{-1} for m-Ti$_3$C$_2$/LiF(S$_1$). e) Fresh electrodes, electrodes after f) 200, g) cycles, h) 1200 cycles at 300 mA g^{-1} for Ti$_3$C$_2$.
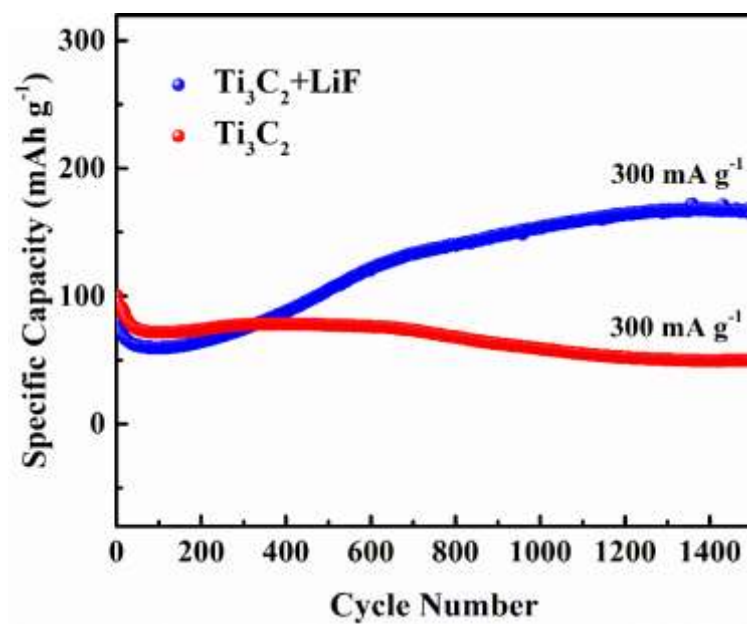
Figure S11. Long-term cycling performance of Ti_3C_2+LiF (20 wt. %) mixtures and Ti_3C_2 for LIBs at 300mA g^{-1}.
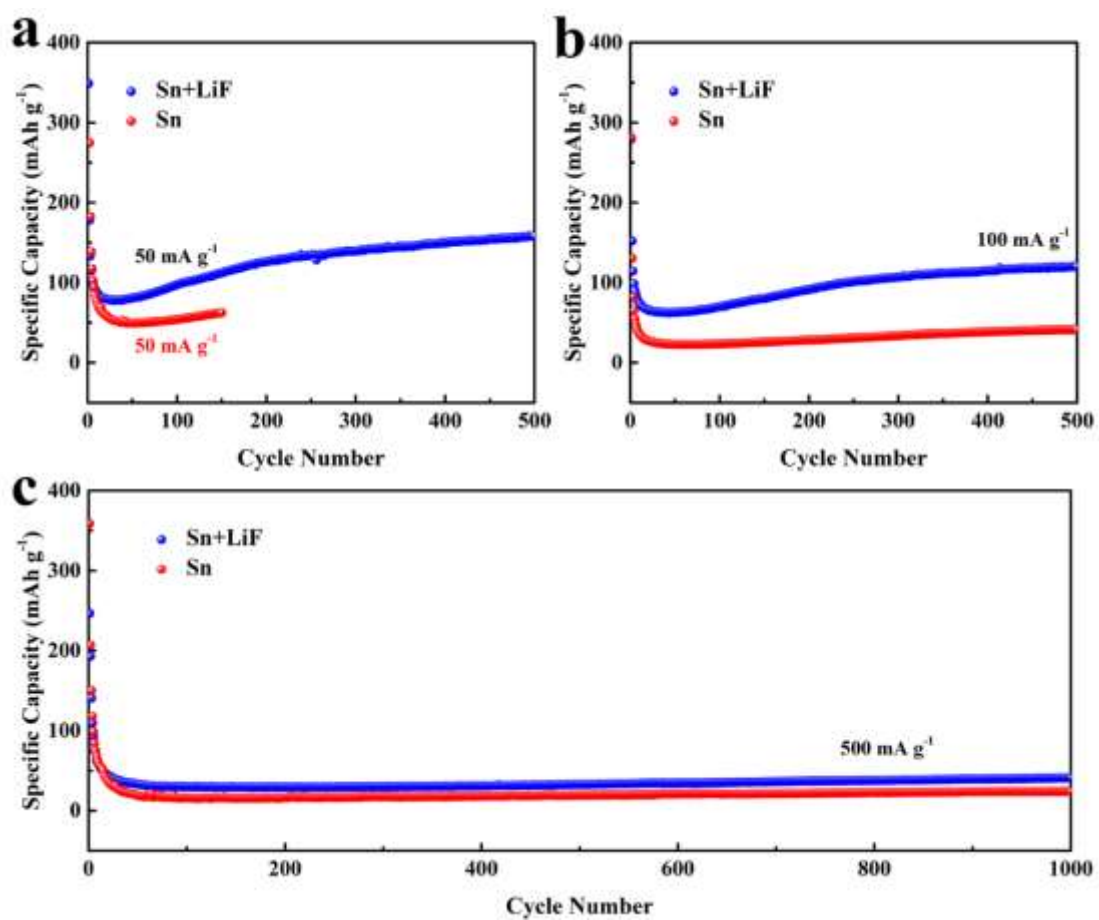
Figure S12. Long-term cycling performance of Sn+LiF (20 wt. %) mixtures and Sn

for LIBs at a) 50, b) 100, c) 500 mA g^{-1}.

Figure S13. Long-term cycling performance of TiO$_2$+LiF (20 wt. %) mixtures and TiO$_2$ for LIBs at at a) 50, b) 100, c) 500 mA g^{-1}.

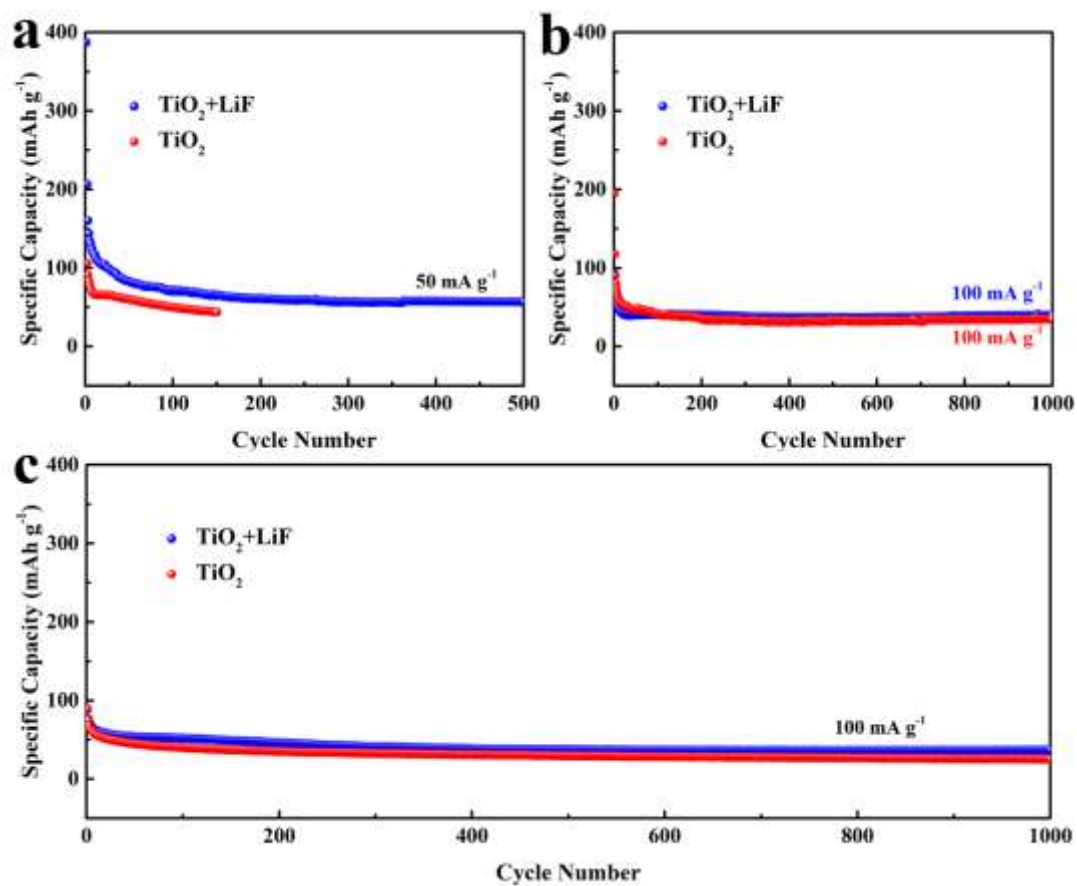**Table S1.** Comparison of the electrochemical performance of various MXene anode materials.

Sample	Current density (mA g^{-1})	Initial discharge capacity (mAh g^{-1})	Cycling number	Reversible discharge capacity (mAh g^{-1})	Capacity retention (%)	Ref
Multi-layered Ti$_2$C	30	475	25	160	33.7	[1]
	300	270	80	110	40.7	
Exfoliated Ti$_3$C$_2$	300	230	150	100	43.5	[2]
Multi-layered Ti$_2$C	26	264.5	75	118.7	44.9	[3]
Delaminated Ti$_3$C$_2$	300	852.2	100	138	16.2	[4]
Multi-layered Ti$_3$C$_2$	20	502.1	100	97.4	19.4	[5]
Multi-layered Ti$_3$C$_2$	180	205				[6]
m-Ti$_3$C$_2$/LiF sediments	300	115	1500	136	118.3	This work
s-Ti$_3$C$_2$+LiF (20 wt. %)	100	580	100	335	57.8	This work

Table S2. Energy dispersive X-ray (EDX) analysis of Ti$_3$C$_2$ etched by HF.

elements	wt %
C	22.29
O	10.83
F	11.75
Al	1.32
Ti	52.81

Table S3. Energy dispersive X-ray analysis (EDX) of m-Ti$_3$C$_2$ in m-Ti$_3$C$_2$/LiF(S$_1$).

elements	wt. %
C	12.05
O	5.99
F	25.28
Al	1.58
Ti	55.09

Table S4. Energy dispersive X-ray analysis (EDX) of m-Ti$_3$C$_2$ in m-Ti$_3$C$_2$/MgF$_2$(S$_2$).

elements	wt %
C	12.98
O	11.37
F	15.54
Al	8.78
Mg	4.89
Ti	46.44

Table S5. The quantitative XPS results of m-Ti$_3$C$_2$/LiF(S$_1$).

elements	at %	wt %
C	24.9	16.6
O	9.6	8.5
Ti	14.2	37.8
Al	0.2	0.3
F	25.5	26.9
Li	25.6	9.9

Table S6. XPS peak fitting results of *m*-Ti$_3$C$_2$/LiF(S$_1$).

		Concentration (%)
Ti 2p	Ti-C	1.74
	Ti^{2+}	22.64
	Ti^{3+}	50.75
	Ti-O	24.87
C 1s	C-Ti	39.14
	C-C	36.56
	C-O	17.62
	O-C=O,C-F	6.68
O 1s	Ti-O	34.75
	C-Ti-O$_x$	42.25
	C-Ti-(OH)$_x$	23

Table S7. XPS peak fitting results of Ti$_3$C$_2$ etched by HF.

		Concentration (%)
Ti 2p	Ti-C	0.87
	Ti^{2+}	26.22
	Ti^{3+}	51.57
	Ti-O	21.34
C 1s	C-Ti	45.04
	C-C	46.47
	C-O	6.54
	O-C=O,C-F	1.95
O 1s	Ti-O	31.5
	C-Ti-O$_x$	57.45
	C-Ti-(OH)$_x$	11.05

Table S8. The electrochemical impendence fitting results and calculated values of $D_{Li}+$ of m-Ti$_3$C$_2$/LiF(S$_1$), Ti$_3$C$_2$ and m-Ti$_3$C$_2$/MgF$_2$(S$_2$).

Samples	Rs (Ω)	Rct (Ω)	$D_{Li}+$ (cm^2 s^{-1})
m-Ti$_3$C$_2$/LiF(S$_1$)	6.4	33	4.9×10^{-16}
Ti$_3$C$_2$	9.5	123	3.4×10^{-16}
m-Ti$_3$C$_2$/ MgF$_2$(S$_2$)	3.5	427	5.5×10^{-17}

References

[1] M. Naguib, J. Come, B. Dyatkin, V. Presser, P.-L. Taberna, P. Simon, M. W. Barsoum, Y. Gogotsi, *Electrochem. Commun.* **2012**, *16*, 61.

[2] O. Mashtalir, M. Naguib, V. N. Mochalin, Y. Dall'Agnese, M. Heon, M. W. Barsoum, Y. Gogotsi, *Nat. Commun.* **2013**, *4*, 1716.

[3] D. Sun, M. Wang, Z. Li, G. Fan, L.-Z. Fan, A. Zhou, *Electrochem. Commun.* **2014**, *47*, 80.

[4] T. Zhang, L. Pan, H. Tang, F. Du, Y. Guo, T. Qiu, J. Yang, *J. Alloys Compd.* **2017**, 695, 818.

[5] N. Sun, B.-y. Yang, J.-c. Zheng, Z.-j. He, H. Tong, L.-b. Tang, C.-s. An, B. Xiao, *Ceram. Int.* **2018**, *44*, 16214.

[6] Y. Li, H. Shao, Z. Lin, J. Lu, L. Liu, B. Duployer, P. O. A. Persson, P. Eklund, L. Hultman, M. Li, K. Chen, X. H. Zha, S. Du, P. Rozier, Z. Chai, E. Raymundo-Pinero, P. L. Taberna, P. Simon, Q. Huang, *Nat. Mater.* **2020**, 19, 894.